ZAAYMAN, J. J. J., and VAN ROOYEN, G. T. The toughness of the heat-affected zone of welds in 11,5 per cent chromium steels. *INFACON 6. Proceedings of the 1st International Chromium Steels and Alloys Congress, Cape Town.* Volume 2. Johannesburg, SAIMM, 1992. pp. 137–142.

The Toughness of the Heat-affected Zone of Welds in 11,5 Per Cent Chromium Steels

J. J. J. ZAAYMAN and G. T. VAN ROOYEN
University of Pretoria, Pretoria, South Africa

The impact properties of the heat-affected zone (HAZ) that develops in low-carbon 11,5 per cent chromium steels during welding are inferior to those of the base material owing to a resultant large grain size and unfavourable transformation products.

The HAZ of four commercially produced 11,5 per cent chromium alloys was simulated when the specimens were subjected to a rapid heating and cooling cycle. The Charpy impact properties of the weld-simulated specimens were determined at different peak temperatures. Specimens subjected to higher peak temperatures in each case resulted in an increase in the ductile-to-brittle transition temperature (DBTT) of each alloy. Despite small differences in the chemical compositions of the alloys used, large differences in impact properties were measured. It was found that small amounts of ferrite are detrimental to the impact properties. Although fully martensitic structures resulted in the lowest DBTT, differences in the lath structure of the martensite also had a marked affect on the DBTT.

Introduction

During the welding of 11,5 per cent chromium stainless steels, the heat-affected zone (HAZ) in the parent metal can be divided into two zones. A high-temperature zone (HTHAZ) develops adjacent to the weld metal where the temperature is sufficiently high to enter the single delta-phase field. Depending on the heat input and the exact chemical composition, the thickness of this zone is restricted and can vary in thickness from 0,2 to 1,0 mm. Owing to the high temperature reached in the HTHAZ, grain growth occurs. Adjacent to the HTHAZ there is a heat-affected zone where the temperature exceeds the lower critical temperature (Ac1) but stays below the upper critical temperature (Ac4). The resultant grain size in this zone is also much smaller than that in the adjacent HTHAZ. An example of the HAZ that develops along the fusion line of a weld in an 11,5 per cent chromium steel is shown in Figure 1.

Generally, the impact properties of the HTHAZ in a ferritic stainless steel are inferior to those of the base material[1]. In practice, the impact properties of this HTHAZ are very difficult to assess, and the impact properties of welds are critically dependent on the exact location of the tip of the notch of Charpy specimens. In the case of 11,5 per cent chromium steel, the true brittleness of this HTHAZ is not usually measured because of the protection provided by the adjacent much softer, ductile austenitic weld metal. Specially designed test specimens[2] are required for an evaluation of the true impact properties of the HTHAZ.

This paper describes the work undertaken to elucidate the detailed influence of the chemical composition. To avoid the complication associated with the interpretation of the impact properties of the HAZ in actual welds, the HAZ properties can best be assessed by simulation of the temperature cycle

FIGURE 1. The HAZ along the fusion line in an 11,5 per cent chromium steel

to which the HAZ is subjected during welding[3]. By variation of the peak temperature and time at temperature, and by control of the rate of heating and cooling, the microstructure can be reproduced at any position in the HAZ of a weld. Because a uniform microstructure that extends over at

least 10 mm can be obtained by such a simulated heat treatment, a study can be made of the inherent impact properties of a steel at various positions along the HAZ of a weld.

Simulation of the HAZ

A transformer was used to pass a heavy electric current through a specimen clamped between water-cooled electrodes to simulate the thermal cycle experienced by different parts of the HAZ during welding. A schematic diagram of the apparatus that was used is shown in Figure 2. The current that was necessary to simulate the high heating rate was controlled by means of an auto-transformer. To ensure reproducible conditions, the current was terminated at the desired peak temperature with a relay system, after which the specimen was allowed to cool naturally, most of the heat being conducted away by the water-cooled electrodes.

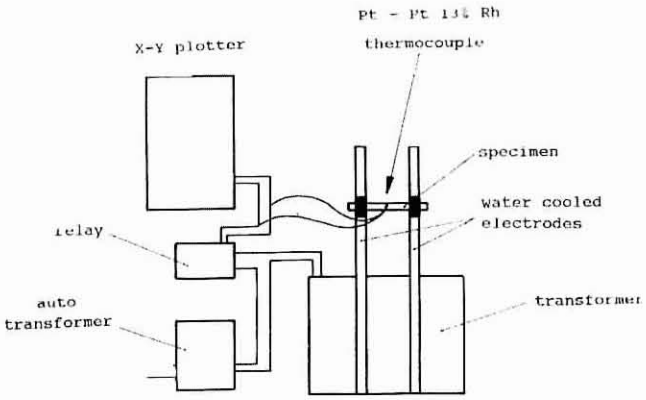

FIGURE 2. Schematic diagram of the HAZ simulator

The electrical current was controlled to give the same heating rate (160 °C per second) that the HAZ of a 5 mm thick plate will experience during welding, based on the temperature–time profiles of Ashby and Easterling[4]. The cooling rate was controlled so that the cooling time between 800 and 500 °C in the simulated HAZ corresponded to that of an actual weld produced by a heat input of 2,5 kJ/mm. The cooling rate was controlled by variation in the distance between the two water-cooled electrodes. To simulate the structure of the HAZ some distance from the fusion line, it is necessary not only to use lower peak temperatures but also to lower the heating and cooling rates[5].

Five different peak temperatures were used to simulate the microstructure of different portions of the HAZ. These temperatures, which are shown in Figure 13, were selected to be just below the Ac1 temperature (830 °C), well within the stability zone of the austenite phase (1000 °C), below and above the Ac4 temperature (1125 °C and 1295 °C), and well within the stability zone of the delta-ferrite phase (1380 °C) close to the liquidus temperature. The liquidus temperatures of the different alloys used were determined by heating until melting occurred. These temperatures varied between 1430 and 1450 °C. Testing was limited to a peak temperature of 1380 °C to ensure that local melting did not occur during the simulation process. Comparison of the microstructure of a simulated HAZ with that of an actual weld adjacent to the fusion line showed close correspondence.

The heating and cooling rates, and the peak temperatures, were perfectly reproducible, the recorded peak temperatures differing by less than ±1 °C. A record of a simulated thermal cycle is shown in Figure 3.

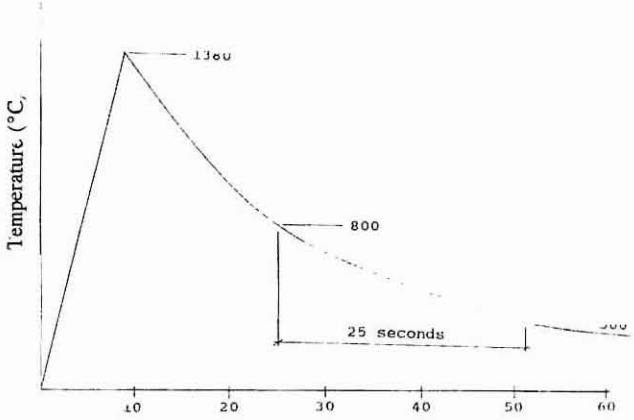

FIGURE 3. Temperature–time profile recorded during simulation to a peak temperature of 1380 °C

Experimental Procedure

Charpy impact specimens were prepared from rolled sheets of four different commercially produced 11,5 per cent chromium alloys. The chemical compositions of the alloys are shown in Table I. The alloying elements not shown are virtually the same for all the alloys. The specimens were prepared with the specimen axis along the rolling direction, and the notch machined through the thickness perpendicular to the rolling direction (crack divider orientation). The specimens were 5 mm thick and were machined according to ASTM standard E 23-82 for sub-sized specimens.

TABLE I
THE CHEMICAL COMPOSITIONS OF THE SPECIMENS AND CERTAIN TRANSFORMATION PROPERTIES DERIVED DURING WELD SIMULATION

Element	D	C	B	A
C	0,025	0,022	0,023	0,021
S	0,004	0,006	0,006	0,006
P	0,018	0,023	0,027	0,030
Mn	1,04	**0,49**	0,98	0,94
Si	0,39	0,41	0,40	0,87
Cr	**11,10**	**11,07**	**11,55**	**12,18**
Ni	**0,46**	**0,85**	**0,19**	**0,17**
Nb	0,003	0,005	0,004	**0,286**
N	0,0197	0,0154	0,0138	0,0324
Ac1	815	835	825	–
Ac4	1200	1200	1170	–
M_S	445	445	390	–
FF	7,9	8,0	10,0	14,0

Kaltenhauser ferrite factor (FF) = %Cr + 6%Si + 8%Ti + 4%Mo + 2%Al + 4%Nb – 2%Mn – 4%Ni – 40% (C + N)

A minimum of 8 specimens were used for every simulation temperature. The V-notch for the impact tests was machined after the simulated heat-treatment cycle. The ductile-to-brittle transition temperature (DBTT), equivalent to an impact energy of 25 J for standard-size specimens, was determined by Charpy impact testing. After the impact testing, one half of each specimen was sectioned along the rolling direction for metallographic and hardness (HV 30) examination. For this purpose, the specimens were alternately polished and etched to reveal the grain boundaries and transformation products, a modified Kalling's no. 2 etchant being used.

In the determination of fracture modes, the fracture surfaces of the impact specimens were examined by scanning electron microscopy (SEM).

During the simulated heat treatment, differential thermal analysis was used in the determination of the dynamic temperatures for Ac1 (ferrite to austenite start), Ac 4 (austenite to delta-ferrite start), and M_S (martensite start) of the different alloys during the rapid heating and cooling cycles. The technique relies on the enthalpy change associated with a phase transformation.

For this purpose, the instantaneous rate of heating or cooling was obtained by differentiation of the temperature signal by means of an electronic differentiator. The critical temperature of a phase change was determined from inflections in the heating and cooling rate curves on an X–Y recording as shown in Figure 4.

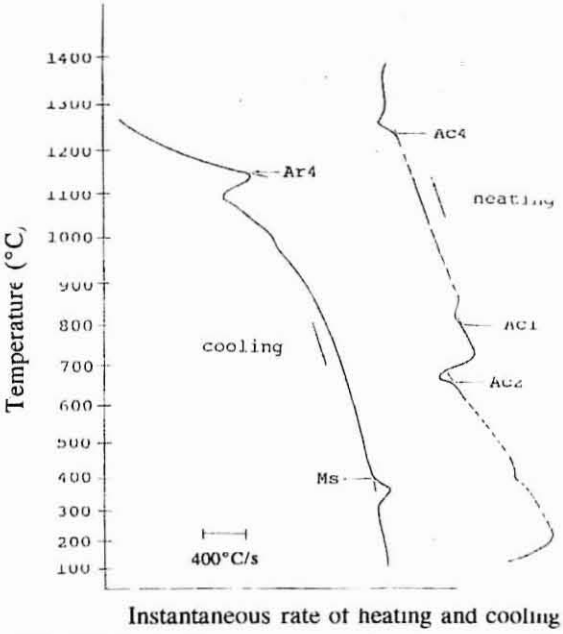

FIGURE 4. Graph of temperature versus instantaneous rate of heating and cooling for an 11,5 per cent chromium specimen, showing the onset of different phase transformations during weld simulation.

Results

Impact Properties

There are marked differences in the impact properties of the different alloys that were simulation-treated to the same peak temperature. The Charpy impact properties at a peak simulation temperature of 1380 °C are shown in Figure 5.

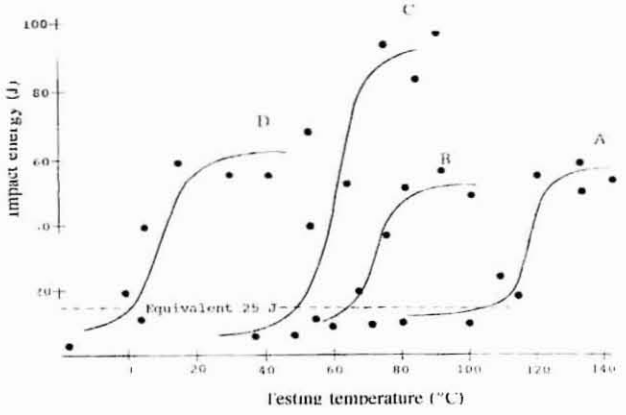

FIGURE 5. Charpy impact energy as a function of testing temperature after simulation to a peak temperature of 1380 °C

For simulation treatments at lower peak temperatures, the equivalent 25 J DBTTs versus the peak temperatures during simulation are shown in Figure 6.

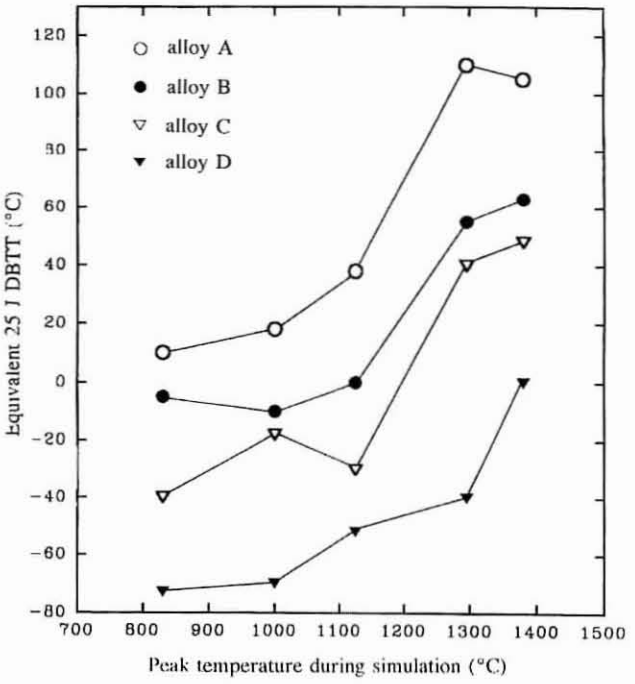

FIGURE 6. The influence of the peak simulation temperature on the equivalent 25 J DBTT

Microstructure

Microstructures after the simulation are shown in Figure 7.

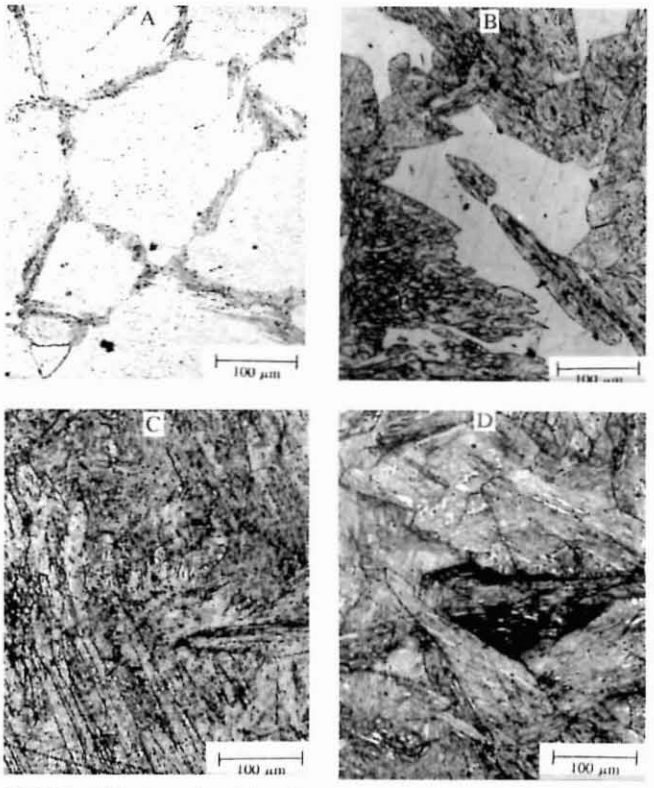

FIGURE 7. Photographs of the microstructures after simulation to 1830 °C

Alloy A was ferritic throughout the thermal cycle, with the exception of small amounts of grain-boundary austenite that formed during cooling and that was transformed to martensite on cooling below the martensite temperature.

After simulation to a peak temperature of 1380 °C, alloy B had a duplex structure consisting of 40±5 per cent ferrite and 60±5 per cent martensite as determined by point-counting analyses. The other two alloys, C and D, had fully martensitic structures, with less than 5 per cent ferrite in alloy D.

Grain Size

It is well known that an increase in the ferrite grain size usually results in an increase in the DBTT[6]. The increase in the ferrite grain size of alloy A as a result of simulation treatment at higher peak temperatures is shown in Figure 8. The inferior impact properties of this alloy after high-temperature simulation can be attributed to an excessive ferrite grain size.

The average ferrite grain size resulting from the simulation treatment to a peak temperature of 1380 °C was about 360 μm.

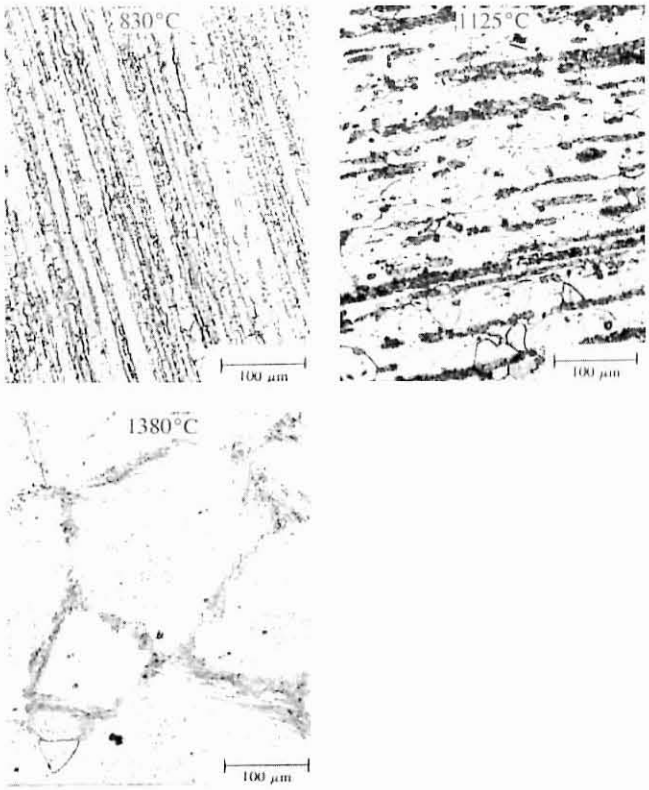

FIGURE 8. Photographs of the microstructure of alloy A after simulation to 830 °C, 1125 °C, and 1380 °C

In the case of the martensitic structures, the DBTT properties are only indirectly related to the grain size of the austenite from which the martensite forms. In the case of alloys B, C, and D, it was difficult to determine the austen*ite* grain size unequivocally. At the highest simulation temperature, the grain size varied between 70 and 110 μm and could not be directly related to the impact properties.

Fractography

In the case of alloy A, fractographic examination by SEM showed that the grain-boundary martensite fractured by microvoid coalescence (dimples) characteristic of a ductile fracture (Figure 9). In this case, the specimen was fractured 10 °C below the equivalent 25 J DBTT, at which temperature the ferrite fractured in a brittle, transgranular-cleavage fracture mode.

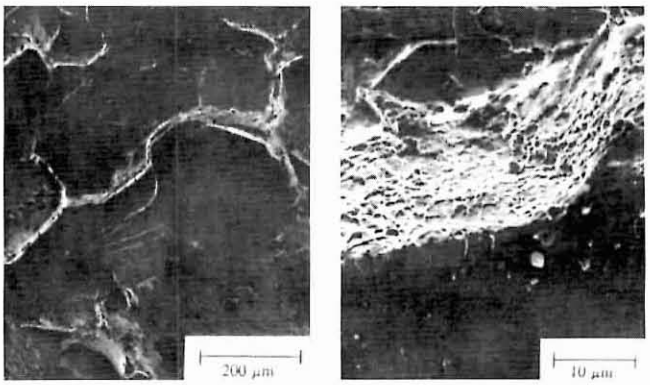

FIGURE 9. SEM fractographs of alloy A fractured at 90 °C

In the case of alloys B, C, and D, the fracture of specimens at the DBTT was in all instances mainly by cleavage. The cleavage facets on the fractured surfaces of alloys B, C, and D are visible on the SEM fractographs shown in Figure 10. The dimensions of the cleavage facets in most cases match the dimensions of the austenite grains.

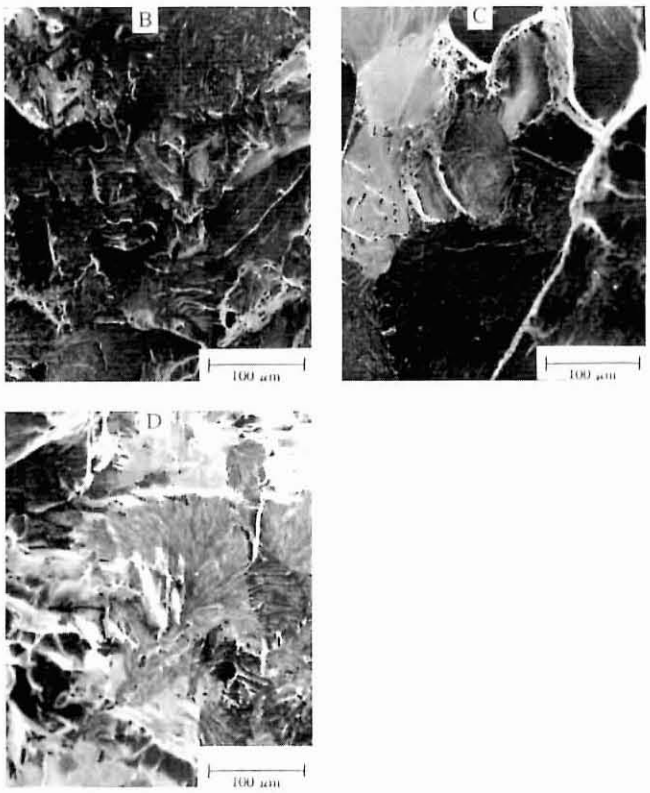

FIGURE 10. SEM fractographs of the fractured surfaces of alloys B, C, and D fractured at the transition temperatures 60, 50, and 0 ° C respectively

Hardness Measurement

Figure 11 shows the variations in hardness with increasing peak simulation temperature. The hardness values for alloy A are much lower owing to a general ferritic structure as against ferritic–martensitic structures in the other alloys.

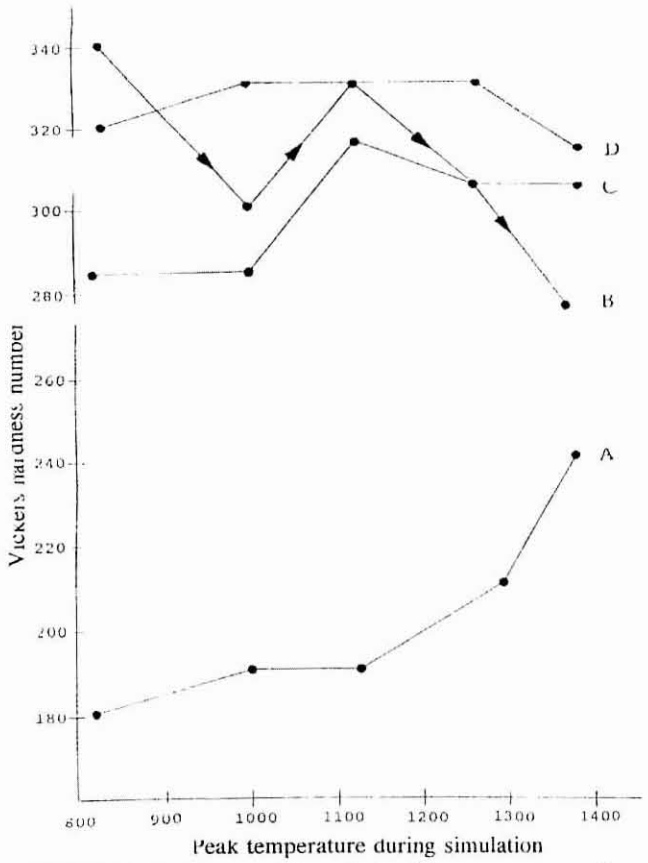

FIGURE 11. The influence of the peak simulation temperature on the Vickers hardness (HV 30) of specimens

The decrease in the simulated HAZ hardness observed in alloys B and D after simulation treatment at the highest peak temperature (1380 °C) is due to the retention of some delta-phase ferrite in the structure. The delta-ferrite in the structure of alloy D was observed only after simulation to a peak temperature of 1380 °C.

Rolling Direction

The properties of alloys B and D, with longitudinal and transverse orientations to the rolling direction, are shown in Figure 12. These specimens were heat-treated by a HAZ simulating cycle with a peak temperature of 1380 °C.

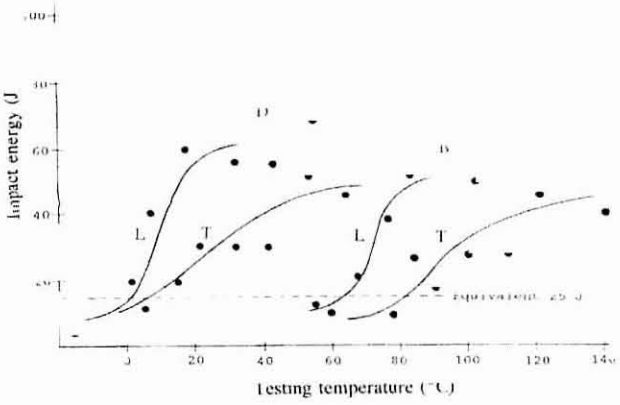

FIGURE 12. Charpy impact energy of alloys B and D after HAZ simulation to a peak temperature of 1380 °C. The results are given for specimens with a longitudinal (L) and transverse (T) orientation to the rolling direction

In both alloys, the transition from brittle to ductile behaviour occurred over a greater temperature interval for specimens with a transverse orientation. This behaviour is typical for rolled material[7]. Despite this difference, the equivalent DBTT of alloy D was unaffected. In the case of alloy B, which contained some delta-ferrite, the DBTT for the longitudinal and transverse orientation differed by 20 °C.

Chemical Composition

There are no major differences in the chemical compositions of the four alloys. However, the minor differences in the concentrations of the alloying elements, highlighted in Table I by the bold print, was sufficient to result in different amounts of martensite and ferrite in the final microstructures. The higher chromium and niobium contents of alloy A resulted in an almost fully ferritic structure, with only minor quantities of grain-boundary martensite.

The relatively large amount of niobium in alloy A resulted in the formation of niobium carbo-nitride precipitates, which probably pinned the grain boundaries at low peak simulation temperatures. Solutions of these precipitates at higher peak simulation temperatures[4] probably led to the abnormal grain growth and the resulting large grain size. The equivalent chromium contents or ferrite numbers of alloys C and D were such that martensite was the main constituent after cooling.

Discussion

During actual welding, portions of the HAZ closer to the weld metal would be subjected to higher peak temperatures and higher heating and cooling rates. The increase in the DBTT with increasing peak simulation temperature can therefore be related to the impact properties of the HAZ of an actual weld. Qualitatively, the X-axis of Figure 7 (peak simulation temperature) can therefore be related to the distance along the HAZ of an actual weld. For the same heat input, the width of the zone in the HAZ, which can be expected to be embrittled, would be a maximum for alloy A and a minimum for alloy D. The width of the embrittled zone would also be affected by the heat input, and the smallest embrittled zone can be expected with a minimum heat input.[3]

The phase transformations during HAZ simulation and the resulting structures can be related to a schematic phase diagram shown in Figure 13. There, the Kaltenhauser ferrite factor[8], which is an empirical formula relating the influence of different alloying elements on the stability of ferrite, was used as a parameter of the chemical composition. A higher ferrite factor indicates greater ferrite stability, and consequently less austenite will form during cooling after a simulation heat treatment. Less martensite is therefore expected in the HAZ after cooling to room temperature.

The gamma loop on the schematic phase diagram in Figure 13 shifts to higher temperatures and to the left during high heating rates as the Ac1 and Ac4 temperatures, determined during a simulation treatment (Table I), indicate. Alloy B was therefore cooled through the dual phase (delta-ferrite + austenite), and subsequently a large amount of delta-ferrite was retained in the final structure. In the case of alloy A, the dynamic Ac1 and Ac4 temperatures could not be established accurately as a result of the low percentage transformation that occurred during the rapid heating and cooling cycle.

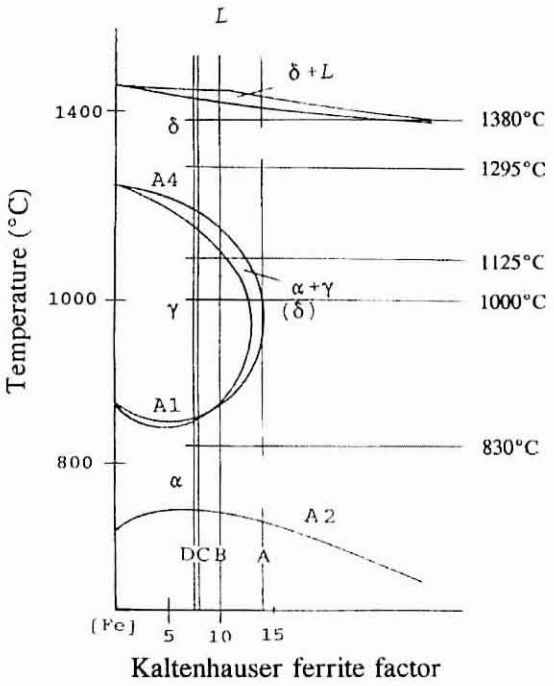

FIGURE 13. Schematic phase diagram with the calculated ferrite factor (FF) as a compositional parameter

The small amount of retained delta-ferrite in the structure of alloy D after a peak simulation temperature of 1380 °C (in comparison with 1295 °C, which gave a fully martensitic structure) resulted in a comparatively large increase in the DBTT. This indicates that even small amounts of delta-ferrite are detrimental to impact properties[9].

Usually, the presence of martensite in the HAZ of a weld influences the impact properties negatively by initiating fracture[3,9,10]. However, in very-low-carbon 11,5 per cent chromium steels, the martensite that forms is comparatively soft and ductile in comparison with martensite with a higher carbon content[11]. The austenite which nucleated on the delta-ferrite grain boundaries eventually transforms to comparatively tough martensite on these grain boundaries[3]. This is borne out by the fractographs shown in Figure 9, which indicate a ductile (micro-void coalescence) fracture mode for the grain-boundary martensite in comparison with the cleavage of the ferrite. Increasing amounts of martensite in the structure cause an increase in hardness and, consequently, in the stress to which the remaining delta-ferrite is subjected, increasing the probability of cleavage. Increasing amounts of martensite, therefore, do not result in a proportional decrease in the DBTT.

Even in the case of fully martensitic structures (alloys C and D simulated at 1295 °C), there were still large differences in the DBTT. Differences in the austenite grain structures and in the martensite substructure (lath width and packet size), as well as the presence of retained austenite on lath boundaries[12], could affect the DBTT of a fully martensitic structure.

The martensite substructure of alloy D, for example, was much finer than that of alloy C after simulation treatments to the same peak temperature. The SEM fractographs of alloys C and D showed larger cleavage facets on the fractured surface of alloy C.

Conclusions

The heat treatments that simulated the HAZ of welds in low-carbon 11,5 per cent chromium steels showed a progressive increase in the DBTT as simulation was carried out to higher peak temperatures. However, there were large differences in the DBTT in steels of similar chemical composition but significantly different ferrite factors. The presence of small amounts of ferrite in the structure was detrimental, and acceptable DBTTs were attained only when the HAZ had a fully martensitic structure. Even in the case of fully martensitic structures, there were still important differences in the DBTT, which can be related to the prior austenite grain size and the fine substructure of the martensite (lath width and packet size). The state of the carbon and nitrogen, which was not clear in this instance, can also have a significant influence on the impact properties. The results nevertheless indicate that it is possible to produce low-carbon 11,5 per cent chromium steel with acceptable toughness in the HAZ after welding if close control is exercised over the composition.

Acknowledgments

The authors thank Middelburg Steel & Alloys (Pty) Ltd for providing the materials and financial support.

References

1. Thomas, R.C., and Apps, R.L. (1980). Weld heat affected zone properties in AISI 409 ferritic stainless steel. In *Toughness of ferritic stainless steels.* ASTM. S.T.P. 706, Lula, R.A., (ed.), pp. 161-183.
2. Grobler, C. (1987). Weldability studies on 12% and 14% chromium steels, PhD thesis, University of Pretoria.
3. Gooch, T.G., and Ginn, B.J. (1988). Heat affected zone toughness of MMA welded 12% Cr martensitic–ferritic steels. Report to members of The Welding Institute 373, Abington Hall, Cambridge, UK.
4. Ashby, M.F., and Easterling, K.E. (1982). A first report on diagrams for grain growth in welds. *Acta Metall.*, 30, pp. 1969-1978.
5. Lancaster, J.F. (1987). *Metallurgy of welding.* 4th edition, Allen & Unwin (Publishers) Ltd, London, UK. p. 50.
6. Owen, W.S., Whitmore, D.H., Cohen, M., and Averbach, B.L. (1957). *Weld. J.*, 36, pp. 503-511.
7. Dieter, G.E. (1988). *Mechanical metallurgy.* SI metric edition, McGraw-Hill Book Co., pp. 480-481.
8. Kaltenhauser, R.H. (1971). *Met. Eng. Quarterly,* 11, 4, pp. 41-47.
9. Folkhard, E. (1988). *Welding metallurgy of stainless steels.* Springer Verlag, New York, pp. 172-176.
10. Kim, B.C., Lee, S., Kim, N.J., and Lee, D.Y. (1991). Microstructure and local brittle zone phenomena in HSLA steel welds. *Metall. Trans.* A, 22, pp. 139-149.
11. Dolby, R.E. (1976). Factors controlling weld toughness – the present position, The Welding Institute, *Report* no. 14/1976/M, Abington, 150 pp.
12. Tomita, Y. (1991). Development of fracture toughness of ultra high strength low alloy steels for aircraft and aerospace applications. *Mat. Sci. and Tech.*, pp. 481-489.